Arch. Metall. Mater. **65** (2020), 2, 653-666

DOI: 10.24425/amm.2020.132804

W. WOŁCZYŃSKI[1*]

PATTERN SELECTION IN THE EUTECTIC GROWTH – THERMODYNAMIC INTERPRETATION

The (Zn) – single crystal strengthened by the E = (Zn) + $Zn_{16}Ti$ eutectic precipitate is subjected to directional growth by the *Bridgman's* system and current analysis. Experimentally, the strengthening layers (stripes) are generated periodically in the (Zn) – single crystal as a result of the cyclical course of precipitation which accompanies the directional solidification. These layers evince diversified eutectic morphologies like irregular rods, regular lamellae, and regular rods. The L – shape rods of the $Zn_{16}Ti$ – intermetallic compound appear within the first range of the growth rates when the irregular eutectic structure is formed. Next, the branched rods transform into regular rods and subsequently the regular rods into regular lamellae transitions can be recorded. The regular lamellae exist only within a certain range of growth rates. Finally, the regular rods re-appear at some elevated growth rates.

A new solution to the diffusion equation is provided to describe the micro-field of the solute concentration in the liquid adjacent to the front of the growing eutectic structure. The solution is based on the mass balance in the considered system. Moreover, the existence of the protrusion of the leading eutectic phase over the wetting one is required by the mass balance. The appearance of the d – protrusion in the growing eutectic is well confirmed by the experimental observations of the frozen solid/liquid interface. The mentioned solution satisfies the concept of the eutectic *coupled growth* according to which undercooling of the leading phase is less than undercooling of the wetting eutectic phase. Also, the Ti – solute micro-segregation / redistribution is analyzed within the matrix of the single crystal. The micro-segregation is described as a result of the solution to the adequate, newly developed differential equation. The definition for the solute redistribution is given by the subsequently / separately formulated relationship. This definition takes into account both extent -, and intensity of the solute redistribution.

Finally, the entropy production is calculated for the regular lamellae -, and for the regular rods formation, respectively. The entropy production is a function of some parameters which define the eutectic phase diagram, coefficient of the diffusion in the liquid, and some capillary parameters connected with the mechanical equilibrium located at the triple point of the solid/liquid interface. Branches formation is related to the marginal stability. A new criterion is formulated and subjected to successful verification. It is: ***in the structural – thermodynamic competition the winner is this kind of the pattern for which minimum entropy production has a lower value***

Keywords: Criterion of lower minimum entropy production,Structural competition,Marginal Stability, Irregular growth, Microsegregation

Notations

d – protrusion of the leading phase above the wetting phase, [m],
D – coefficient of diffusion in the liquid, [m^2/s],
k – partition ratio, [at.%/at.%],
N – solute concentration, [at.%],
N_E – eutectic concentration of titanium, [at.%],
N_0 – nominal solute concentration in a given alloy, [at.%],
r_α – half the radius of the α – eutectic phase rod, [m],
r_β – sum of the half the radius of the α – eutectic phase rod and the width of the β eutectic phase (matrix), [m],
S_α – half the width of the α – eutectic phase lamella, [m],
S_β – half the width of the β – eutectic phase lamella, [m],
t – time, [s],
T – temperature, [K],
v – crystal growth rate, [m/s],
ε – amplitude of the s/l interface perturbation, [m],
λ_{SL} – critical wavelength of perturbation generated at the s/l interface, [m],

1. Introduction

The growth of the (Zn) single crystal strengthened by the E = (Zn) + $Zn_{16}Ti$ precipitate was performed by the *Bridgman's* system. Experimentally, the strengthening layers (stripes) are

[1] INSTITUTE OF METALLURGY AND MATERIALS SCIENCE, POLISH ACADEMY OF SCIENCES, 30-059 KRAKÓW, 25 REYMONTA STR., POLAND

* Corresponding author: w.wolczynski@imim.pl

generated periodically in the (Zn) – single crystal as a result of the cyclical course of precipitation which accompanies the directional solidification. These layers evince diversified eutectic morphologies like irregular rods, regular lamellae, and regular rods. Transformations of the mentioned structures (one into other) were observed at some threshold growth rates. It is obvious that the eutectic structures formation is subjected to the competition.

Thus, it is postulated that the thermodynamics of irreversible processes is able to explain / justify the structural transformations. For that reason, a new criterion is formulated to describe eutectic morphologies competition which results in the appearance of the wining structure.

The criterion is: ***in the structural – thermodynamic competition the winner is this kind of the pattern for which minimum entropy production is lower***.

An application of such a criterion requires to calculate the entropy production per unit time for both eutectic regular structures: lamellar structure and rod-like structure. Subsequently, the entropy production is to be subjected to minimization in order to formulate the so-called *Growth Law* for considered structures.

The (Zn) – single crystal growth proceeds in a stationary state in the *Bridgman's* system with constant both the v – growth rate and $G = \partial T/\partial z$ – thermal gradient. Thus, the application of the theorem of *minimum entropy production* can be assumed in this situation.

After some rearrangements and in a general form, [1,2], entropy production per unit time and unit volume associated with the mass transfer only is given as follows:

$$\sigma_D = \frac{DR_g\,\psi}{N_i\left(1-N_i\right)}\left|grad.N_i\right|^2 \quad T \equiv T_{s/l} = const. \tag{1}$$

R_g is the gas constant, ψ – thermodynamic factor, and $T_{s/l}$ – temperature of the solid / liquid interface.

Eq. (1) is ready to be introduced into Eq. (2) in order to calculate entropy production per unit time, separately for lamellar -, and rod-like eutectic structure formation within the layers strengthening the (Zn) – single crystal.

$$P_D = \int_V \sigma_D\, dV \tag{2}$$

The current description is connected with the mass transfer in the liquid adjacent to the s/l interface but contained in the diffusion zone: $z_D \approx D/v$ (in the z – direction). Entropy production associated with the heat transfer is neglected, ($\sigma_T = 0$).

The V – volume is the key parameter for the subsequent calculation / solution of the integral, Eq. (2). It leads to the separation of integration which now, will be made simultaneously for the lamellar -, and rod-like structure formation. The V – volume has already been defined for the lamellar -, and the rod-like structure formation, [2].

The V – volume is reproduced periodically in the regular eutectic morphology. However, this volume is not the same for every new solidification rate. Therefore, the average entropy production is to be calculated, [2]:

a) for the lamellar eutectic growth

$$\overline{P}_D^L = \frac{1}{S_\alpha + S_\beta}\int_V \sigma_D\, dV \tag{3a}$$

b) for the rod-like eutectic growth

$$\overline{P}_D^R = \frac{1}{\pi\left(r_\alpha + r_\beta\right)^2}\int_V \sigma_D\, dV \tag{3b}$$

Next, Eq. (4) is obtained by introducing Eq. (1) into Eq. (2):

$$P_D = \frac{DR_g\,\psi}{N_i\left(1-N_i\right)}\int_V \left|grad.N_i\right|^2 dV \tag{4}$$

According to the thermodynamics of irreversible processes, the stationary state is defined by the criterion of *minimum entropy production*, [3]. Thus, the application of this criterion allows for defining the size of the regular eutectic structure.

The eutectic transformation proceeds under the stationary state in such a way that the regular lamellae / rods, growing at an imposed thermal gradient and a constant solidification rate, evince inter-phase spacing (λ, R) which corresponds to the minimum entropy production.

Therefore, the mathematical optimization of the regular morphology formation described by the entropy production leads to the formulation of the so-called *Growth Law* for lamellar or rod-like structure, respectively, [4].

Additionally, application of the concept of marginal stability, [5], to define the *operating range* for the irregular eutectic structure formation will be shown in the next chapter.

Moreover, descriptions of both irregular – into regular structure transformation (debranching), and regular rod-like -, into regular lamellar structure transformation will be delivered.

Finally, examination of the newly developed theory for the solute micro-field formation with the verification of the local mass balance which allows to display the leading phase protrusion will be performed.

The entropy production per unit time and unit volume, Eq. (1), has been determined for the isothermal s/l interface. The geometry of this isothermal interface should be bound with the shape of the transition layer, [6,7].

Finally, calculation of the entropy production per unit time, Eq. (4), was performed for the $0 \le z \le z_D$ – boundary layer, where, $z_D \approx D/v$, [4].

Calculation of the entropy production per unit time, Eq. (4), is currently limited to the entropy production associated with the mass transfer only. It is self-explanatory because heat transfer runs very quickly in comparison with the mass transfer. Thus, contribution of the heat transfer to the entropy production is negligible, [8].

2. Irregular eutectic growth

Irregular eutectic growth has been observed in the strengthening layer of the (Zn) – single crystal for the $0 < v \le v_1$ – growth rates range, [2]. Certain models for irregular eutectic structure

formation are based on the diffusion in the liquid and the s/l interface undercooling, [9], and [10].

The current model shows the possibility to adapt two thermodynamic conditions to the description of irregular structure growth. It is justified because two extremely different types of morphology can be selected. First, the eutectic structure with the maximum perturbation of the *non-faceted* phase interface could be distinguished. Second, the regular eutectic structure (in some areas well visible within generally irregular morphology) would also be exposed. The first structure is associated with state of marginal stability, while the second one refers to stationary state, Fig. 1.

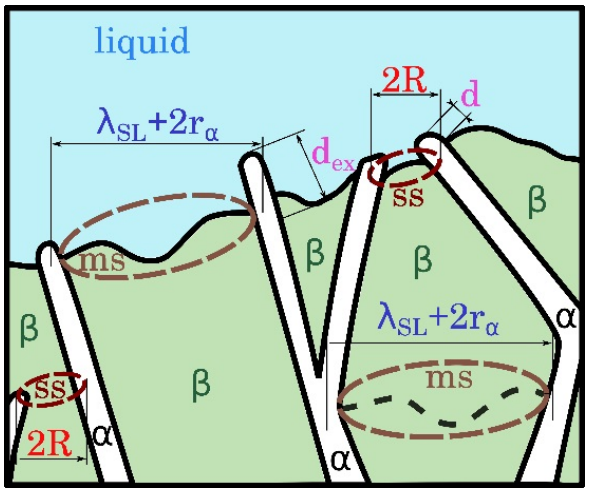

Fig. 1. Model for the irregular eutectic structure formation; distinguished: the *ms* – marginal stability, and the *ss* – stationary state; the d_{ex} – excess protrusion (referred to the appearance of the δT_K – kinetic undercooling of the s/l interface of the *faceted*, leading phase; α – *faceted* eutectic phase, β – *non-faceted* eutectic phase; dashed line – former state of the marginal stability state

It is assumed in the current model that the structure formation oscillates between the stationary state and the marginal stability, Fig. 1. Thereby, this oscillation phenomenon evokes the existence of a whole spectrum of the interphase spacing. So the appearance of the spacing spectrum occurs within the *operating range* of the growth rates, although the growth rate (crucible displacement rate imposed on the *Bridgman's* system) is constant during the experiment under investigation. The areas of the regular structure are formed with the same rate as the crucible displacement rate, but the branched structure is growing with the less intense rate. Thus, an average spacing can be subjected to the structural analysis within the supposed *operating range*.

The scheme shown in Fig. 1 was primarily designed for one of the first models for the irregular structure growth, [9]. Usually, the so-called *operating range* was associated with the geometry of the perturbed interface of the *faceted* phase, [10]. Yet, some experimental observations of the frozen *s/l* interface do not confirm the existence of this perturbation, [11]. For this reason, the existence of this perturbation has been removed from the current model / scheme, whereas regular and *excess* protrusions of the leading, *faceted* phase have been introduced, Fig. 1.

In the analyzed irregular eutectic growth, some fluctuations of the solute concentration are connected with the phenomenon of branching and resultant perturbation of the real solute concentration field, $\delta\left(\delta N^L(x,z)\right)$, and $\delta\left(\delta N^L(r,z)\right)$, respectively. The fluctuation / perturbation occurs in the direct neighborhood of the stationary state, Fig. 1. This fluctuation gives rise to the appearance of the so-called *excess* entropy production.

In these areas (branching regions) of the irregular eutectic morphology formation, the system rotates around the stationary state which is essentially associated with the regular structure which forms locally at the *minimum entropy production*.

In the current model, a marginal stability is assumed to control the maximum fluctuation of the solute concentration field and resultant maximum perturbation of the *s/l* interface shape. Both states (stationary state and marginal stability) are selected in the generally irregular structure, Fig. 1. At the marginal state, corresponding to the transition between stability and instability, the *excess* entropy production vanishes, [5], and the mentioned perturbations do not develop. The wavelength of the considered perturbation is assumed to be equal to the λ_{SL} – wavelength, Fig. 2.

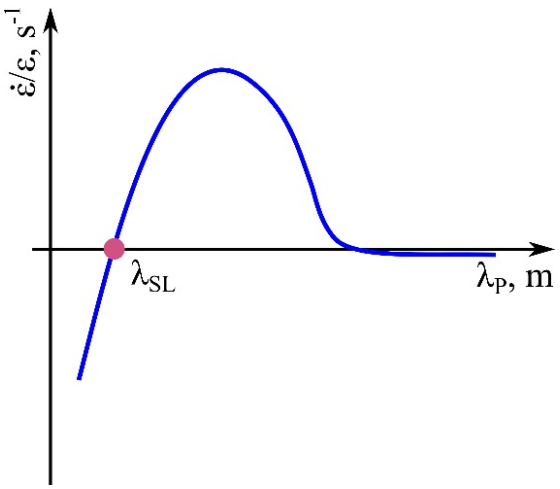

Fig. 2. Interface's tendency to instability (rate of perturbation propagation) versus the λ_p – wavelength of the perturbation, shown schematically according to the stability / instability theory, [12], which is adapted for the description of branching, [13]

The λ_{SL} – wavelength introduced into the scheme, Fig. 1, is defined as follows:

$$\lambda_{SL} = 2\pi\left[\Gamma_\beta / \left(m_\beta G_C - G\right)\right]^{0.5} \tag{5}$$

with, Γ_β – the *Gibbs-Thompson's* parameter for the β – *non-faceted* phase, G_C – solute concentration gradient at the *s/l* interface of the β – *non-faceted* phase, G – thermal gradient at the s/l interface of the β – *non-faceted* phase, [13].

The structural analysis of the strengthening layer situated in the (Zn) – single crystal allows to reveal both extreme situations: a) the moment when the regular eutectic structure is formed, b) the moment when the maximal wavelength of the perturbation appears, Fig. 3.

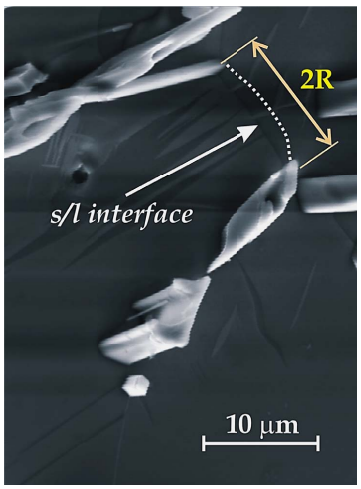

Fig. 3a. Frozen *s*//*l* interface of the (Zn) – eutectic phase; the juxtaposed speculative dotted line is plotted to show the expected, fully parabolic, interface shape; $0 < v \le v_1$

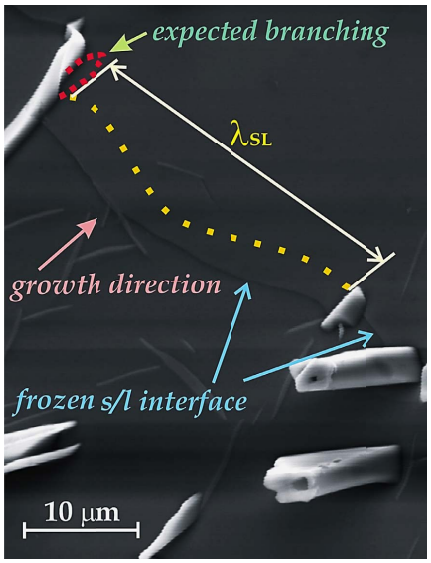

Fig. 3b. Almost fully shaped perturbation developed on the *s*//*l* interface of the (Zn) – *non-faceted* phase (juxtaposed – speculative, dotted line showing possible position of the λ_{SL} – wave; marked – expected branching of the $Zn_{16}Ti$ – *faceted* phase); $0 < v \le v_1$

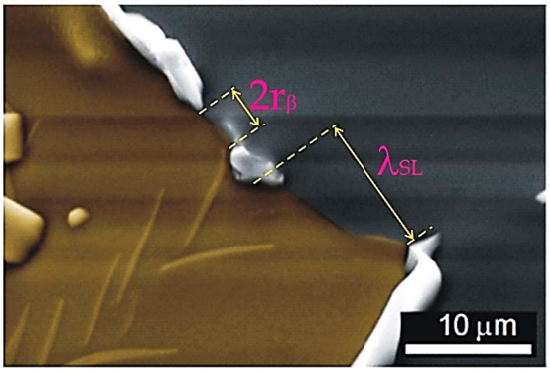

Fig. 3c. Co-existence of the *ss* – state with the parabolic s/l interface of the (Zn) – *non-faceted* phase (locally regular structure) and *ms* – state with the marginally perturbed *s*//*l* interface of the (Zn) – *non-faceted* phase (new color superposed over the frozen solid to make the *s*//*l* interface well-marked)

The eutectic transformation proceeds under the stationary – marginal state in such a way that the irregular lamellae / rods, growing at an imposed thermal gradient and a constant rate of the macroscopic s/l interface displacement, but within the operating range of the local growth rates, evince average inter-phase spacing ($\hat{\lambda}$, or $\hat{R}$) which results from the λ, or R interphase spacing associated with the minimum entropy production of a given stationary state and λ_{SL} – wavelength of perturbation connected with the rotation around this state.

It is important for the current model, that the state of marginal stability can be located on the paraboloid of entropy production drawn for both generalized thermodynamic forces, X_T, X_C (that is, drawn in the "thermodynamic" coordinate system), [14]. Therefore, the above statement can be illustrated by means of this paraboloid shown in Fig. 4.

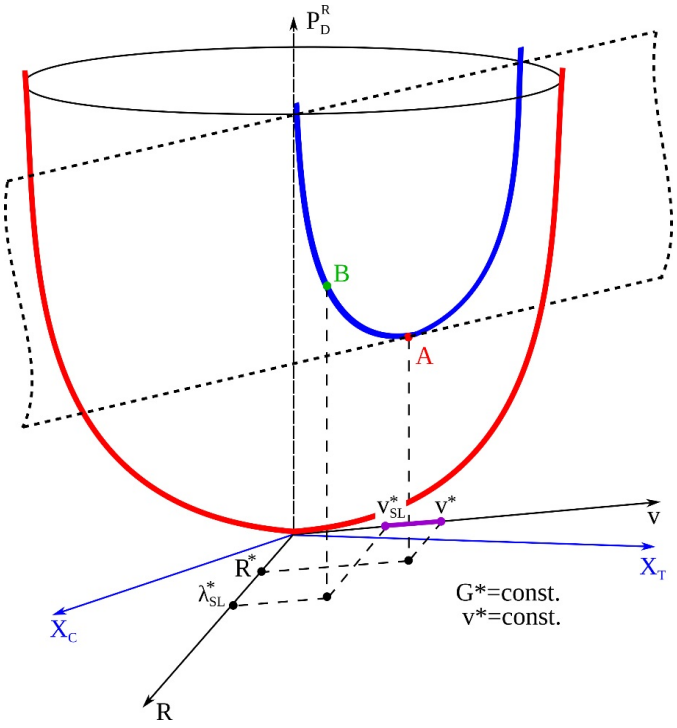

Fig. 4. Illustration of the appearance of the whole spectrum of the interphase spacing as a result of the thermodynamic oscillation between two extreme points: A – stationary state with *minimum entropy production* (local minimum of the paraboloid), and B – marginal stability for the imposed both G^* – thermal gradient, and v^* – growth rate; selected: R^* – half the inter-rod spacing and corresponding λ^*_{SL} – maximal wavelength of the perturbation of the s/l interface of the *non-faceted* phase

The $v^*_{SL} \Leftrightarrow v^*$ – range, distinguished in Fig. 4, is the *Operating Range* for the irregular structure formation (when the imposed both: G^*, v^* are constant). The paraboloid of the entropy production is transformed from the "thermodynamic" coordinate system (X_T, X_C – generalized thermodynamic forces) into the "technological" coordinate system (v, R) in agreement with the performed integration over the V – volume, Eq. (2), and under simplification / assumption that the paraboloid does not change its shape.

2.1. Irregular / regular structure transformation

The transformation of the branched irregular structure into the regular structure occurs within the $v_1 < v \le v_1'$ – range of growth rates. Thus, it seems reasonable to provide the simplified model / scheme of the irregular structure formation to study the mentioned transformation, Fig. 5.

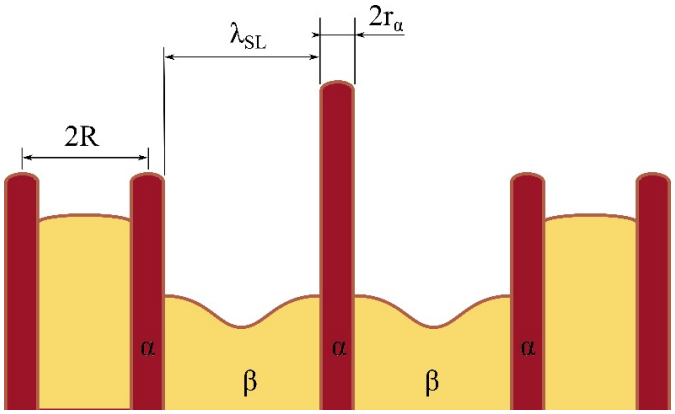

Fig. 5. Simplified model for the irregular structure formation within the $v_{SL} \Leftrightarrow v$ – *operating range*, where v is a given growth rate imposed in the studied experiment and also growth rate of the regular structure in some areas located within generally irregular eutectic morphology, and v_{SL} is a corresponding rate of displacement of the maximally perturbed s/l interface of the (Zn) – *non-faceted* – phase being currently under marginal stability

The simplified scheme of the irregular structure formation allows to formulate a definition for the average interphase spacing. The following definition can be used to describe the growth of the lamellar eutectic structure:

$$\hat{\lambda} = 0.5\lambda + S_\beta + 0.5\lambda_{SL} \tag{6}$$

The irregular -, into regular structure transformation is justified by the following reduction of the above definition, that is: $\hat{\lambda} = 0.5\lambda + S_\beta + 0.5\lambda_{SL} \rightarrow S_\alpha + S_\beta + S_\beta + S_\alpha = \lambda$. The analogous description / reduction can be delivered for the rod-like irregular structure, Fig. 5.

Then, $2\hat{R} = R + r_\alpha + 0.5\lambda_{SL} \rightarrow r_\beta + r_\alpha + r_\alpha + r_\beta = 2(r_\alpha + r_\beta) \Rightarrow 2(S_\beta + S_\alpha) \equiv \lambda$ due to both irregular -, into regular rod-like structure transformation, and subsequently regular rod-like -, into regular lamellar structure transformation, Fig. 6.

2.2. Ti – solute redistribution along the matrix of the (Zn) – single crystal

The differential equation for the solute micro-segregation which appears during solidification accompanied by eutectic reaction is delivered as follows:

$$\frac{dN^L(x;\alpha)}{dx} = \frac{(1-k)N^L(x;\alpha)}{1+\alpha k\, x - x} \tag{7}$$

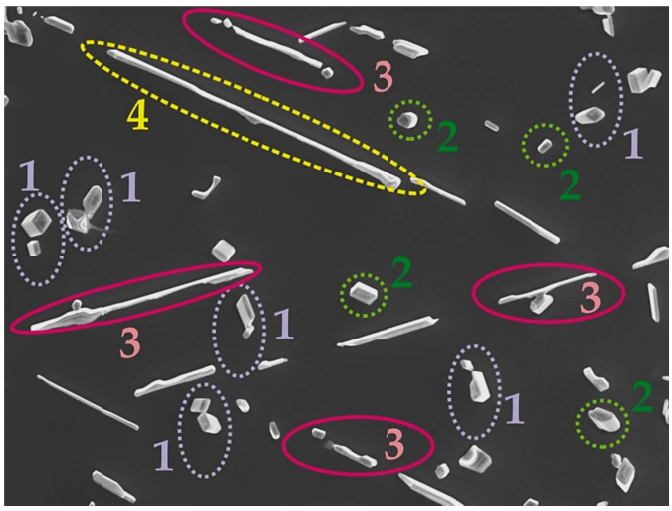

Fig. 6. Co-existence of different forms of the $Zn_{16}Ti$ – compound as observed within the $v_1 \leftrightarrow v_1'$ – range of growth rates: 1) – transformation of irregular branched rods into regular rods (vanishing of branches); 2) – regular rods as a result of the "1" – structural transformation; 3) – transformation of regular rod into regular lamella; 4) – fully shaped regular lamella after the completed transformations, [2]

Thus, the solute concentration in the liquid (solidification path) is:

$$N^L(x;\alpha) = N_0\left(1+\alpha\, k\, x - x\right)^{(k-1)/(1-\alpha k)},$$
$$N^L(0,\alpha) = N_0 \tag{8}$$

$$\alpha = D_S t_l F^{-2} \tag{9}$$

The D_S – diffusion coefficient into the solid, [m^2/s] and t_l – time, [s], necessary for the solidification of the F – matrix length, [m], [2], are applied to the definition of the α – back-diffusion parameter (*Fourier Number*), Eq. (9); x is the current amount of the growing grain (dendrite, cell).

Then, the solute micro-segregation at the moving (and disappearing) s/l interface (s/l interface path) is given as follows:

$$N^S(x;\alpha) = k\, N_0\left(1+\alpha\, k\, x - x\right)^{(k-1)/(1-\alpha k)} \tag{10}$$

Finally, the solute redistribution after back-diffusion (redistribution path) within the solid could be described as:

$$N^B\left(x;X^0,\alpha\right) =$$
$$= \left[k + \beta^{ex}\left(x;X^0\right)\beta^{in}\left(X^0,\alpha\right)\right]N^L(x;\alpha) \tag{11}$$

where, k – partition ratio, [mole fr./mole fr.]; x – current amount of the growing crystal, [dimensionless]; $x = X^0$ – amount of crystal when its growth is arrested and morphology is frozen, [dimensionless]; β^{ex} – coefficient of the redistribution extent, [dimensionless]; β^{in} – coefficient of the redistribution intensity, [dimensionless].

The confrontation of the Ti – solute redistribution (measurement points) with the theoretical solute redistribution is shown in Fig. 7, for the F – matrix length.

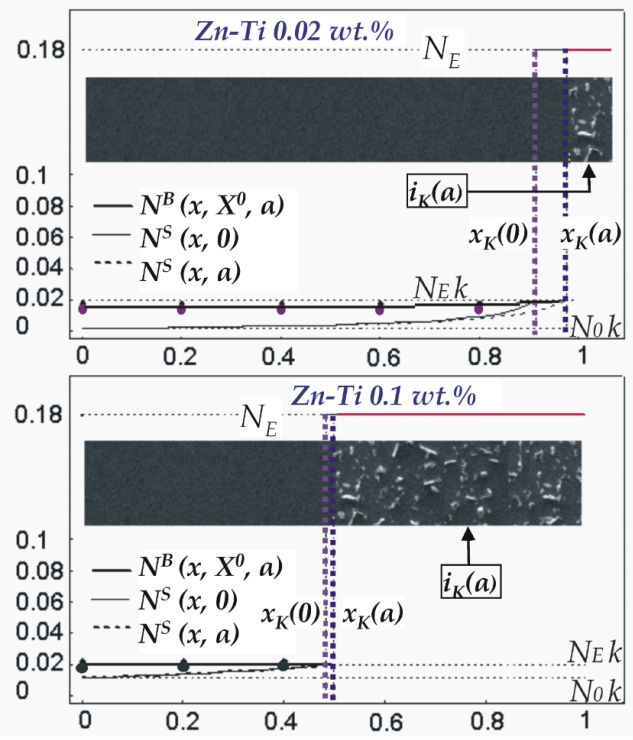

Fig. 7. Ti – solute redistribution (theoretical, as a result of fitting with the use of a suitably chosen back-diffusion parameter, and experimental, as a result of the Ti – solute redistribution measurement (points)); a) for the Zn-0.02Ti -, b) for the Zn-0.1Ti – alloy; red lines show an amount / width of the strengthening eutectic layer versus the x – amount of the growing crystal

As the solute redistribution is the only measurable parameter, the Ti – solute micro-segregation is presented theoretically only, on the basis of calculation of the $N^S(x;0)$ -, and $N^S(x;\alpha)$ – function, Eq. (10), Fig. 7.

The mentioned model allows to calculate the solute redistribution and the amount of eutectic precipitate. Thus, the i_K – total amount of the precipitate, Fig. 8b, is:

$$i_K(\alpha, N_0) = 1 - x_K(\alpha, N_0) \tag{12}$$

$$x_K(\alpha, N_0) = \frac{1}{1-\alpha k}\left[1-\left(N_E / N_0\right)^{\frac{1-\alpha k}{k-1}}\right]$$

$$\text{when } 0 \le \alpha \le \alpha_E(N_0) \tag{12a}$$

$$x_K(\alpha, N_0) = 1 \quad \text{when} \quad \alpha_E(N_0) < \alpha \le 1 \tag{12b}$$

with the definition of the α_E – threshold back-diffusion parameter:

$$\left(\alpha_E\, k\right)^{\frac{k-1}{1-\alpha_E k}} = N_E / N_0 \tag{13}$$

The i_K – total eutectic precipitate consists of the i_E – equilibrium precipitate, $i_E(N_0) = i_K(1, N_0)$, and i_D – non-equilibrium precipitate, $i_D(\alpha, N_0) = i_K(\alpha, N_0) - i_E(N_0)$.

The above model, Eq. (7)-Eq. (13) is reducible to the equilibrium solidification, (EQS in Fig. 8a), and to the Scheil's theory, [15], (SCHEIL in Fig. 8a) and is able to describe the rapid solidification, (RS in Fig. 8a) while taking into account the partition ratio behavior shown schematically in Fig. 8a. Both models can be compared to each other from the viewpoint of the mass balance satisfaction, Fig. 8b.

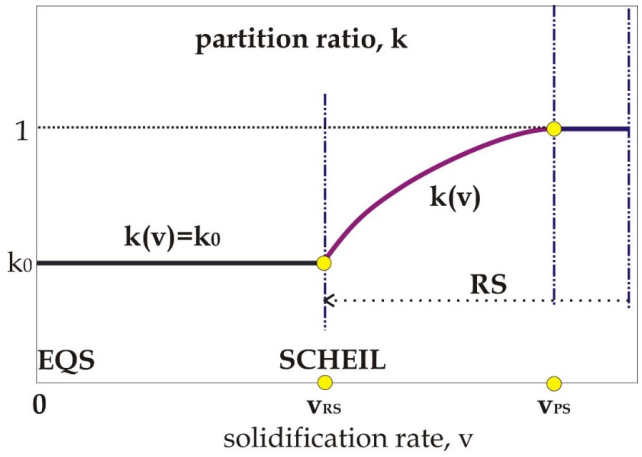

Fig. 8a. Evolution of the partition ratio versus solidification rate according to the current model of the solute segregation / redistribution; k_0 – equilibrium partition ratio, [mole fr./mole fr.]; υ_{RS} – threshold solidification rate (crystal growth rate) just between Scheil's theory application and the beginning of rapid solidification, [m/s]; υ_{PS} – solidification rate (crystal growth rate) above which partition-less solidification occurs only, [m/s]

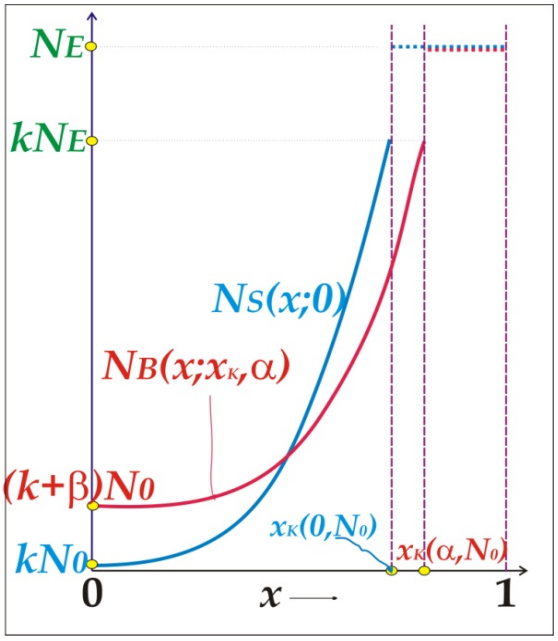

Fig. 8b. Solute redistributions a) according to the Scheil's theory, $N^B(x;0) \equiv N^S(x;0)$, (blue line) and b) according to the current model, $N^B(x;X^0,\alpha) = N^B(x;x_K,\alpha)$, $\beta = \beta^{ex}(x;X^0)\beta^{in}(X^0,\alpha)$, (red line)

When the partition ratio reaches unity above the υ_{PS} – rate then $N^L(x;0) = N_0$, which yields from Eq. (8), solute micro-segregation becomes equal to: $N^S(x;0) = N_0$ (segregation-less solidification, [25]), which yields from Eq. (10), and solute redistribution becomes equal to: $N^B(x;X^0,0) \equiv N^S(x;0) \equiv N^L(x;0) = N_0$, as it yields from Eq. (11) with the coefficient of the redistribution

extent $\beta^{ex}(x;X^0) = 0$ (according to its definition: $\beta^{ex}(x;X^0) = k(1-k)(X^0-x)/(1+kX^0-X^0)$, [16]).

The back-diffusion parameter, (*Fourier Number*), Eq. (9) evolution is presented in Fig. 9, in agreement with the current model of the solute segregation / redistribution. It is evident that the current model of solute redistribution can be developed for multi-component alloys according to the modification mode analyzed in [26].

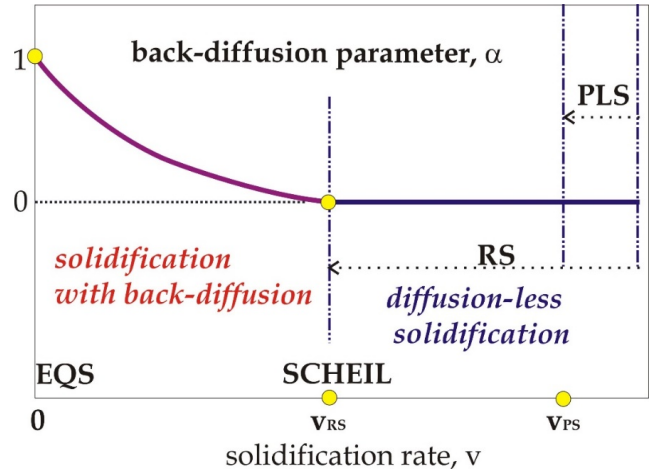

Fig. 9. Evolution of the back-diffusion parameter versus solidification rate according to the current model of the solute segregation / redistribution; v_{RS} – threshold solidification rate (crystal growth rate) just between Scheil's theory application and the beginning of rapid solidification, [m/s]; v_{PS} – solidification rate (crystal growth rate) above which partition-less solidification occurs only, (PLS), [m/s]

The current model, can be referred to the Aziz's theory, [17] on the basis of partition ratio behavior, Fig. 10.

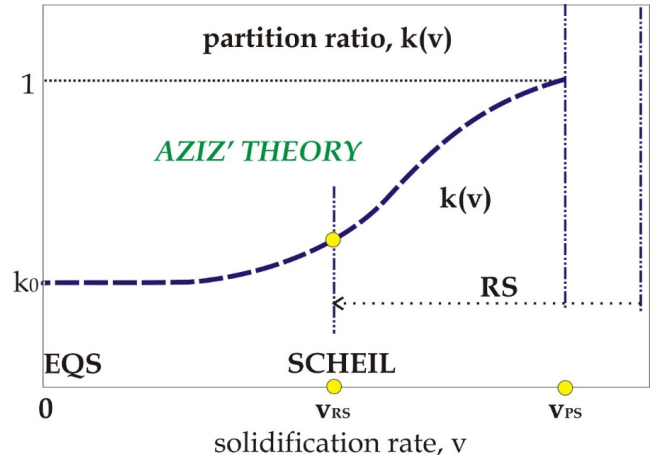

Fig. 10. Evolution of the partition ratio versus solidification rate according to the Aziz's theory, [17], as shown hypothetically in relation to the current model

2.3. Protrusion of the strengthening phase

The quite recent solution to the diffusion equation for the lamellar eutectic growth is delivered under assumptions of the existence of both mechanical equilibrium at the triple point of the *s/l* interface and thermodynamic equilibrium which advances ahead of the α/β – interphase boundary at the steady state, [18].

This steady state solution to the diffusion equation:

$$\frac{\partial^2 \delta N^L}{\partial x^2} + \frac{\partial^2 \delta N^L}{\partial z^2} + \frac{v}{D}\frac{\partial \delta N^L}{\partial z} = 0,$$

is obtained for the liquid adjacent to the α – phase, and to the β – phase, separately:

a) for the α – eutectic phase formation (the $Zn_{16}Ti$ – phase in the Zn – Ti system),

$$\delta N^L(x,z) = \sum_{n=1}^{\infty} A_{2n-1}\cos\left(\frac{(2n-1)\pi x}{2S_\alpha}\right)\exp\left(-\frac{(2n-1)\pi}{2S_\alpha}z\right) \quad (14a)$$

$$A_{2n-1} = -\frac{4}{(2n-1)\pi}\int_0^{S_\alpha} f_\alpha(x)\cos\left(\frac{(2n-1)\pi x}{2S_\alpha}\right)dx \quad n = 1, 2, \ldots$$

b) for the β – eutectic phase formation (the (Zn) – phase in the Zn – Ti system),

$$\delta N^L(x,z) = \sum_{n=1}^{\infty} B_{2n-1}\cos\left(\frac{(2n-1)\pi(x-S_\alpha+S_\beta)}{2S_\beta}\right)\exp\left(-\frac{(2n-1)\pi}{2S_\beta}z\right) \quad (14b)$$

$$B_{2n-1} = -\frac{4}{(2n-1)\pi}\int_{S_\alpha-S_\beta}^{S_\alpha} f_\beta(x)\cos\left(\frac{(2n-1)\pi(x-S_\alpha+S_\beta)}{2S_\beta}\right)dx \quad n = 1, 2, \ldots$$

where, f_j – function used in the boundary conditions, [mole fr.], ($j = \alpha, \beta$), respectively; x, z – geometrical coordinates, [m]; $\delta N^L(x,z)$ – difference between the $N^L(x,z)$ – varying solute concentration, and the N_E – eutectic concentration of the solute.

The above solution ensures the satisfaction of the local mass balance, Eq. (15), under condition that the strengthening phase protrusion, *d*, is taken into account, Fig. 11.

$$\int_0^{S_\alpha} \delta N^L(x,0)\,dx + \int_{S_\alpha}^{S_\alpha+S_\beta} \delta N^L(x,d)\,dx = 0 \quad (15)$$

The local mass balance, Fig. 11, corresponds well with the phase diagram, Fig. 12, illustrating the eutectic coupled growth, $\Delta T_\alpha \neq \Delta T_\beta$, assumed in the model, [18].

The protrusion of the eutectic leading phase (strengthening phase), predicted theoretically, Fig. 11, and observed experimentally [19,20,27] has also been exposed within the layers containing the ((Zn) + $Zn_{16}Ti$) eutectic, Fig. 13. The higher is growth rate, *v*, the smaller is protrusion, *d*:

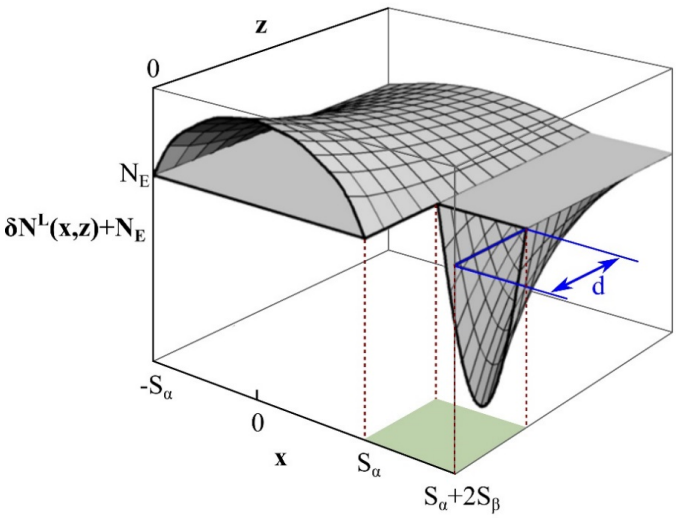

Fig. 11. Local mass balance within the solute concentration micro-field for the lamellar growth as associated with the Eq. (15) validity

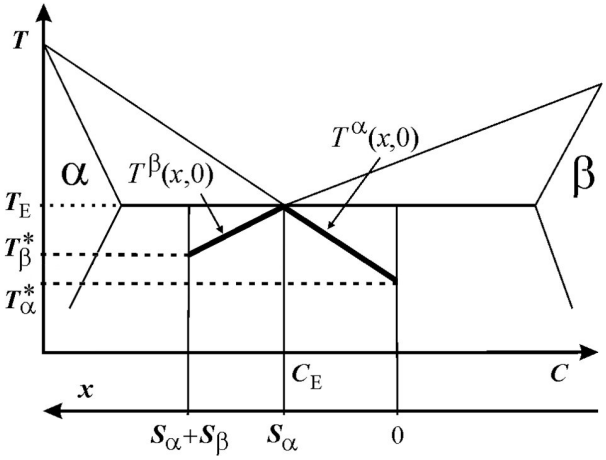

Fig. 12. Arbitrary phase diagram illustrating the coupled eutectic growth; T_α^* – real temperature at the s/l interface of the growing α – phase; T_β^* – real temperature at the s/l interface of the growing β – phase; undercooling: $\Delta T_\alpha = T_E - T_\alpha^*$; $\Delta T_\alpha = T_E - T_\beta^*$

$$\sum_{n=1}^{\infty} A_{2n-1}\frac{(-1)^{n-1}}{(2n-1)}\left(1-\frac{S_\alpha}{S_\beta}\exp\left(-\frac{(2n-1)\pi}{2S_\beta}d\right)\right)=0,$$

$$B_{2n-1}=A_{2n-1}\left(\frac{S_\alpha}{S_\beta}\right)^2,\quad n=1,2,... \qquad (16)$$

Eq. (16) can be supported by the use of a proper *Growth Law*, $(S_\alpha + S_\beta) = f(v)$, [4]. Similar analysis could be developed for the rod-like structure formation, Fig. 13.

2.4. Structural – thermodynamic competition within the strengthening layer

As confirmed experimentally, four ranges of growth rate: $0 \leftrightarrow v_1$; $v_1 \leftrightarrow v_1'$; $v_1' \leftrightarrow v_2$, and $v_2 \leftrightarrow v_3$, are selected for the different patterns appearance on the basis of the performed ob-

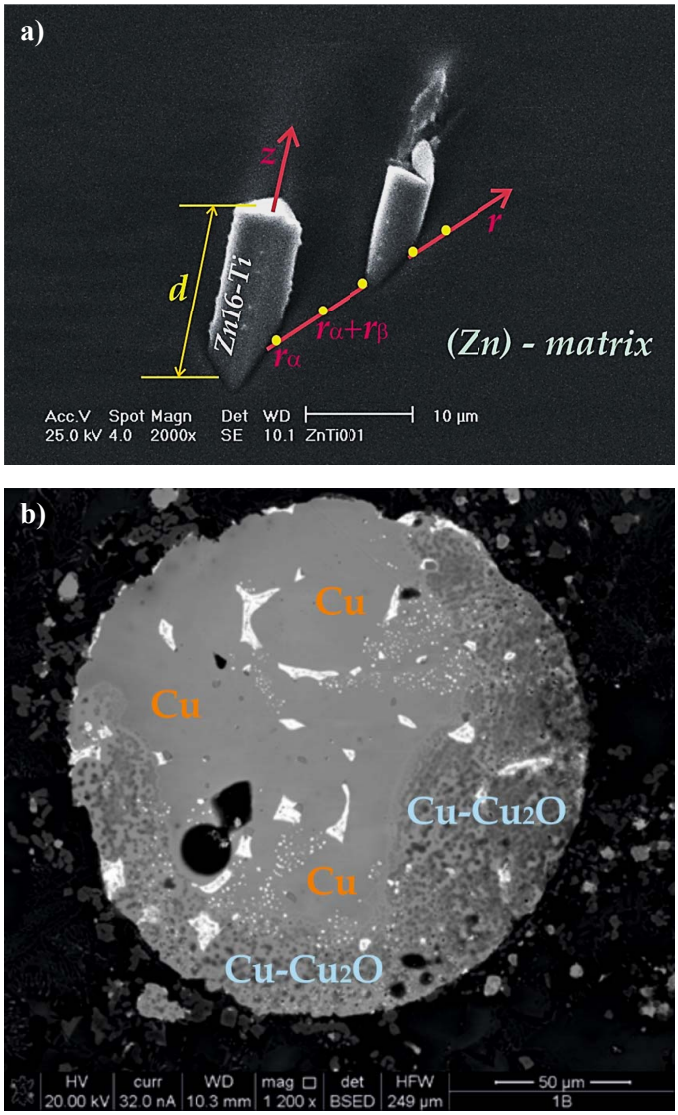

Fig. 13. Observations of the eutectic structure; a) the $Zn_{16}Ti$ – phase protrusion revealed in the strengthening layers (the EDS analysis); the r,z – coordinate system presents situation of the Ti – solute concentration micro-field, d – parameter (leading phase protrusion) is determined / exposed as a result of the (Zn) – single crystal growth arresting, b) rod-like Cu-Cu_2O eutectic revealed in the coagulated copper droplet (grey – black areas)

servations, [20]. Thus, it is postulated to compare the entropy production calculated for both rod-like -, and lamellar structure formation, [4]. First of all, however, evolution of the mechanical equilibrium situated at the triple point of the s/l interface is to be determined. The evolution of the mechanical equilibrium is a function of the v – growth rate, [4], and accompanied anisotropy of the surface free energies. This evolution involves some changes of the $\sigma^L_{(Zn)}$ – surface free energy of the (Zn) – *non-faceted* phase, and the $\sigma_{(Zn)-Zn_{16}Ti}$ – boundary free energy versus growth rate, Fig. 14.

The values of the $\sigma^L_{(Zn)}$ -, $\sigma^L_{Zn_{16}-Ti}$ -, Fig. 14, and additionally estimated, value of the $\sigma_{(Zn)-Zn_{16}Ti}$ – parameter, have been introduced into calculation of the entropy production calculated previously, [4], for the formation of both regular structures, Fig. 15.

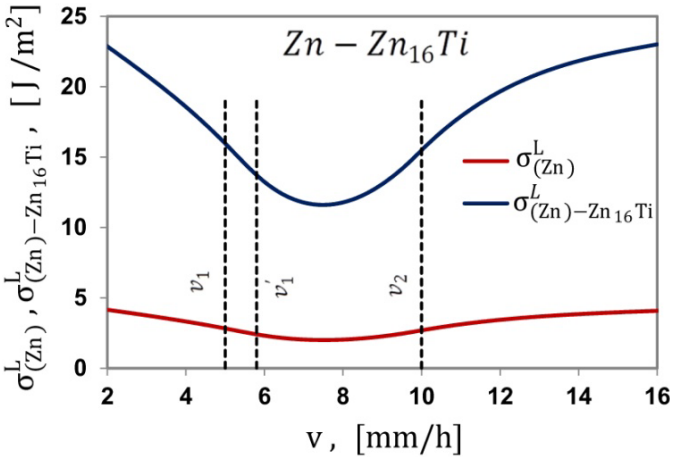

Fig. 14. Changes of the $\sigma^L_{(Zn)}$ – specific surface free energy of the (Zn) – *non-faceted* phase, and the $\sigma_{(Zn)-Zn_{16}Ti}$ – boundary free energy; both parameters determined by a heuristic method with a minimum for lamellar eutectic growth; the $\sigma^L_{Zn_{16}-Ti}$ – specific surface free energy is to be determined with the use of the parallelogram of vectors shown in [4]

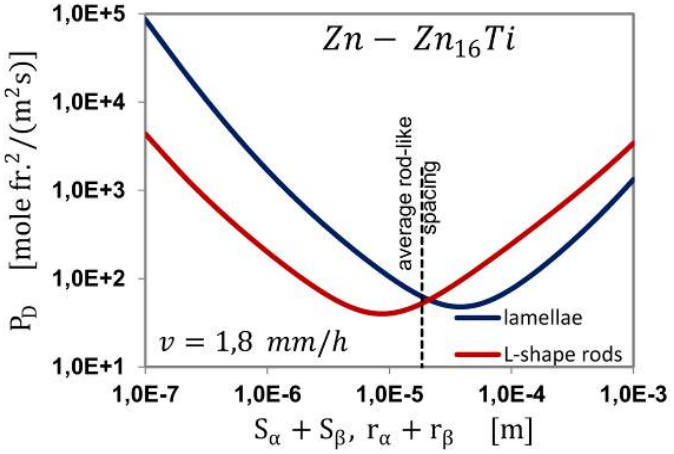

Fig. 15a. Entropy production for the formation of regular, eutectic structures; plotted for the $v = 1.8$ – growth rate, [mm/h]; situation of the $\hat{R}$ – average rod-like spacing; minimum for the rod-like structure formation is situated lower; $0 < v \leq v_1$

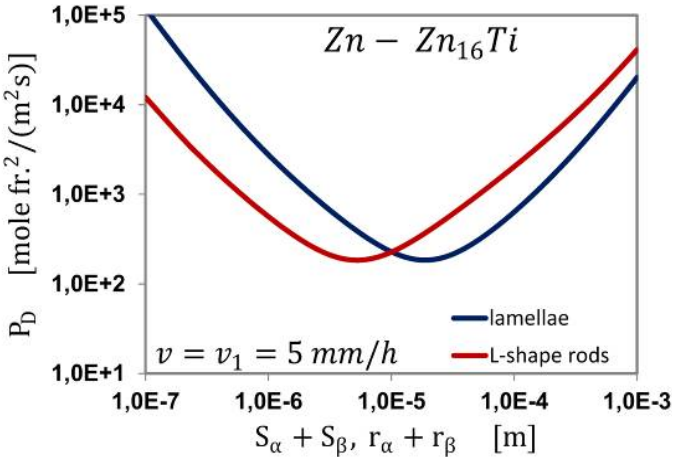

Fig. 15b. Entropy production for the formation of regular, eutectic structures; plotted for the $v = 5$ – growth rate, [mm/h]; both minima are at the same level; transformation of regular rods into regular lamellae expected; $v = v_1$

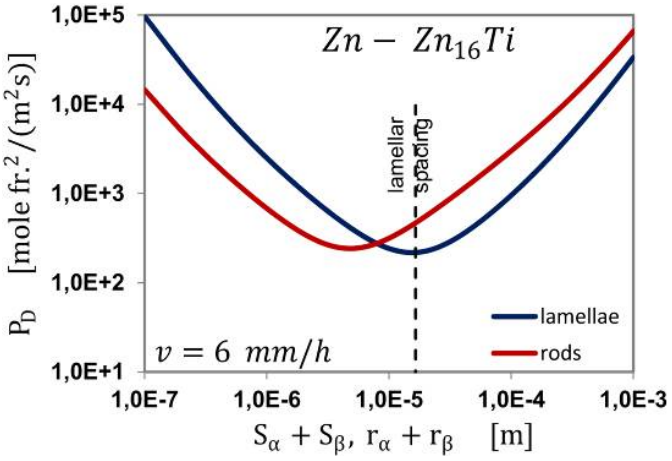

Fig. 15c. Entropy production for the formation of regular eutectic structures; plotted for the $v = 6$ – growth rate, [mm/h]; minimum for the lamellar structure formation is localized lower; $v_1' < v \leq v_2$

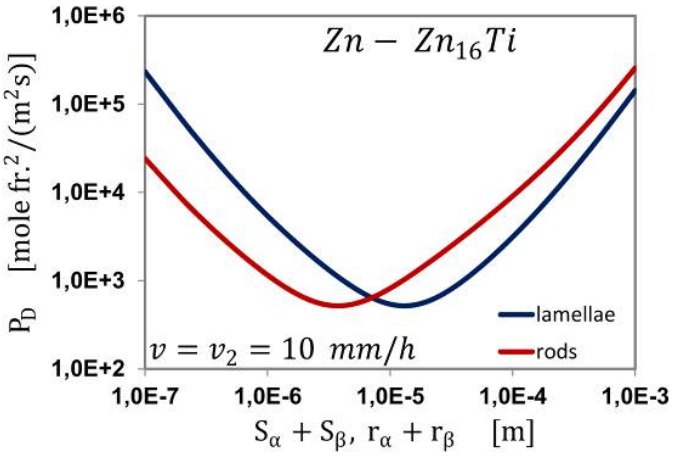

Fig. 15d. Entropy production for the formation of regular eutectic structures; plotted for the $v = 10$ – growth rate, [mm/h]; both minima are at the same level; transformation of regular lamellae into regular rods expected; $v = v_2$

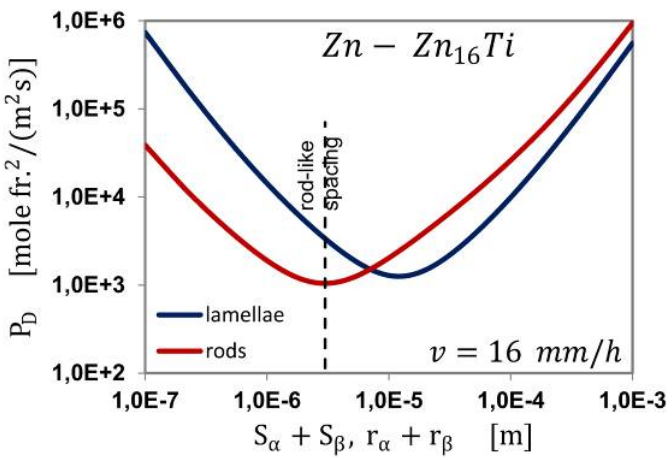

Fig. 15e. Entropy production for the formation of regular eutectic structures; plotted for the $v = 16$ – growth rate, [mm/h]; minimum for the rod-like structure formation is localized lower; $v_2 < v$

Eventually, it is reasonable to gather all the P_D^{min} – minima for both studied structures to present their evolution in function of the v – growth rate, Fig. 16.

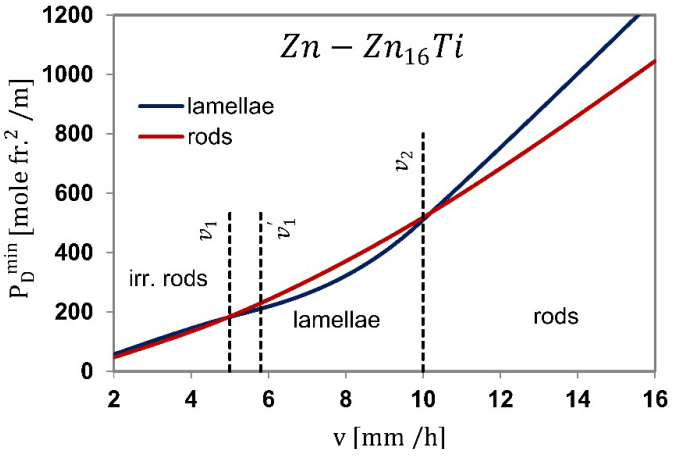

Fig. 16. Values of the *minimum entropy production* for all the ranges of the experimentally imposed rates for the (Zn) – single crystal growth

3. Concluding remarks

The current theory proves that morphological transformations observed within the layers strengthening the (Zn) – single crystal have the thermodynamic background. Since the experiment was performed under stationary state, the only criterion which could be used in such a model is the theorem of *minimum entropy production*. Therefore, entropy production was calculated for the both morphologies formation and subsequently, subjected to the minimization. Then, the application of the postulated criterion: ***in the structural – thermodynamic competition the winner is this kind of the pattern for which minimum entropy production is lower***, has been successfully verified. This verification was obtained by:

a) analysis of the Zn-Zn_{16}Ti phase diagram and some accompanying experiments performed within four ranges of the growth rates,
b) calculation of the entropy production for both examined eutectic structures,
c) development of the *Growth Law* for both eutectic structures appearance,
d) application of the concept of marginal stability to define the *Operating Range* for the irregular eutectic structure formation,
e) descriptions of both irregular – into regular structure transformation (debranching), and regular rod-like -, into regular lamellar structure transformation,
f) examination of the newly developed theory for the solute micro-field formation with the verification of the local mass balance which allows to display the leading phase protrusion.

The entropy production per unit time and unit volume, Eq. (1), has been determined for the isothermal s/l interface. The geometry of this isothermal interface should be bound with the shape of the transition layer, [21].

Calculation of the entropy production per unit time, Eq. (2), is currently limited to the entropy production associated with the mass transfer only. It is self-explanatory because heat transfer runs very quickly in comparison with the mass transfer. Thus, contribution of the heat transfer to the entropy production is negligible, [8].

Moreover, calculation of the entropy production per unit time, Eq. (2), is performed for the $0 \le z \le z_D$ – boundary layer, where, $z_D \approx D/v$.

A deviation from the thermodynamic equilibrium, usually measured as the ΔT – undercooling, is identical for the both eutectic phases, $\Delta T = \Delta T_\alpha = \Delta T_\beta$, in the first approximation. However, calculation of the entropy production allows to apply different real values of undercooling, $\Delta T_\alpha \neq \Delta T_\beta$, [4].

Originally, according to the thermodynamics of irreversible processes, the P_D – entropy production is the function of the X_T – primary thermodynamic force, and the X_C – coupled thermodynamic force, [22]. However, integration, Eq. (4), transforms the calculation of the entropy production from this „thermodynamic" coordinate system into the $(v, S_\alpha + S_\beta)$; $(v, r_\alpha + r_\beta)$ – „technological" coordinate system, [4]. The entropy production plotted in the "thermodynamic" coordinate system has the shape of the paraboloid. Initially, (for simplification) it was assumed that the mentioned paraboloid conserves its geometrical shape in spite of the applied mathematical transformation, $P(X_T, X_C) \rightarrow P(v,(S_\alpha + S_\beta))$; $P(X_T, X_C) \rightarrow P(v,(r_\alpha + r_\beta))$, Fig. 17. However, there is a good prerequisite for plotting a real shape (function) of the entropy production.

A significant advantage of the performed transformation is that the entropy production was integrated over two variables: z, and x, only. This result is in the coupling with the solution to diffusion equation, [6], which is expressed in function of the same variables: z, and x, [4].

Particularly, at the v_K – critical growth rate, perturbation disappears, the regular structure is formed exclusively, and completion of the B $\Rightarrow$ A transition is satisfied.

The A_{MEP} – trajectory contains all the local minima at which the stationary processes can proceed, and B_{MS} – trajectory is bounded with the marginal stability for which the *excess* entropy production reaches zero, $v_{SL}(v) < v$, as $\lambda_{SL}(v) > 2r_\beta(v)$.

Additionally, $2r_\beta > r_\alpha + r_\beta$; $R(v)$ – function, denoted as GL, shows the speculative position of the *Growth Law*, (developed in [4]), plotted, however within the primary coordinate system, X_T, X_C, The MS is speculative position of the corresponding marginal stability.

Not only is the whole spectrum of the inter-phase spacing produced during the (Zn) – single crystal growth (during the system oscillation between the A_{MEP} – trajectory, and the B_{MS} – trajectory) but also is the debranching proceeded continuously in the $v_1 \leftrightarrow v_1'$ – range of growth rates as well. Thus, according to the current experiment, the B $\Rightarrow$ A transition begins at the imposed v_1 – rate and is completed at the imposed v_1' – rate, when the A – attractor is the only state of stability. In reality,

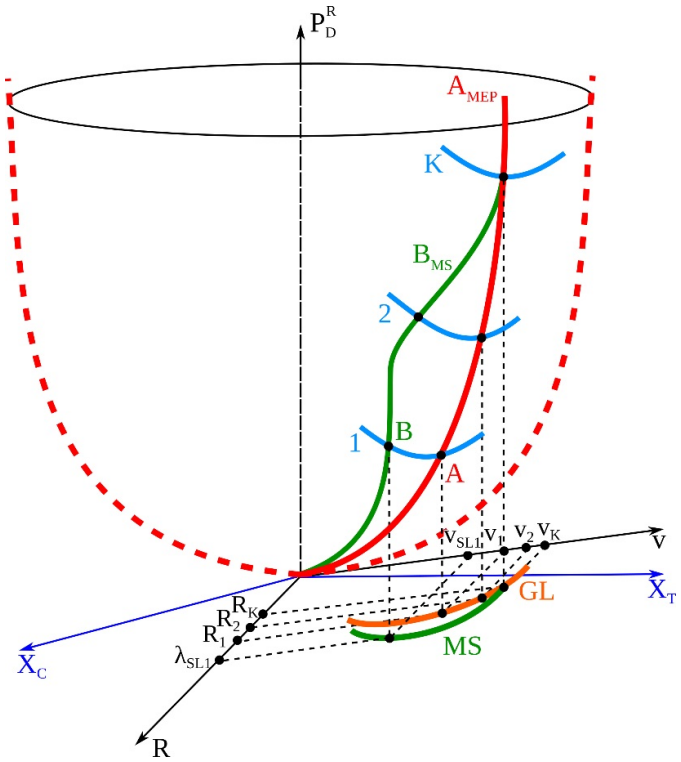

Fig. 17. Paraboloid of the P_D^R – entropy production illustrating the irregular rod-like eutectic growth within the X_T, X_C – coordinate system (the v, R – coordinate system is also incorporated); A – attractor connected with the regular eutectic structure formation at the imposed v_1 – growth rate (R_1 – spacing characterizes the regular structure), and B – bifurcation which appears in the state of marginal stability, at the v_{SL1} – growth rate; analogously, solidification proceeds at the v_2 – growth rate with $R_2(v_2)$ – spacing, and adequate maximal wavelength of perturbation

this is the stationary state as the entropy production reaches the local minimum of the paraboloid under investigation for the v_1' – growth rate. The mentioned structural / thermodynamic oscillation and debranching are shown schematically in Fig. 18.

At the v_1 – growth rate the R_1 – spacing appears (A – attractor), and at the same time, the marginal stability (B – bifurcation located at the maximum of the B_{MS} – marginal stability trajectory) is created at the s/l interface of the *non-faceted* phase moving with the v_{SL1} – rate.

Between the v_1 -, and v_1' – growth rate, the solidification is translating continuously (dashed blue-red line in Fig. 18) from the P_D^R – paraboloid onto the P_D^L – paraboloid of the entropy production.

Within the $v_1' \leftrightarrow v_2$ – range of growth rates the lamellar structure is formed, exclusively (blue line on the A^L_{MEP} – trajectory).

At the v_2 – growth rate the lamellar structure formation is sharply interrupted, and the rod-like regular structure begins to appear immediately (red line on the A^R_{MEP} – trajectory, Fig. 18).

The GL^L -, and GL^R – function show the speculative positions of both *Growth Laws*, (developed in [4]), respectively (plotted, unfortunately, within the "thermodynamic" coordinate system).

The MS – function presents the position of the state of the marginal stability for the irregular eutectic structure formation. It is assumed (for simplification) that the paraboloid of the entropy production drawn schematically in the X_T, X_C – "thermodynamic" co-ordinate system does not change its shape after transformation into the v, λ, or v, R – "technological" co-ordinate system.

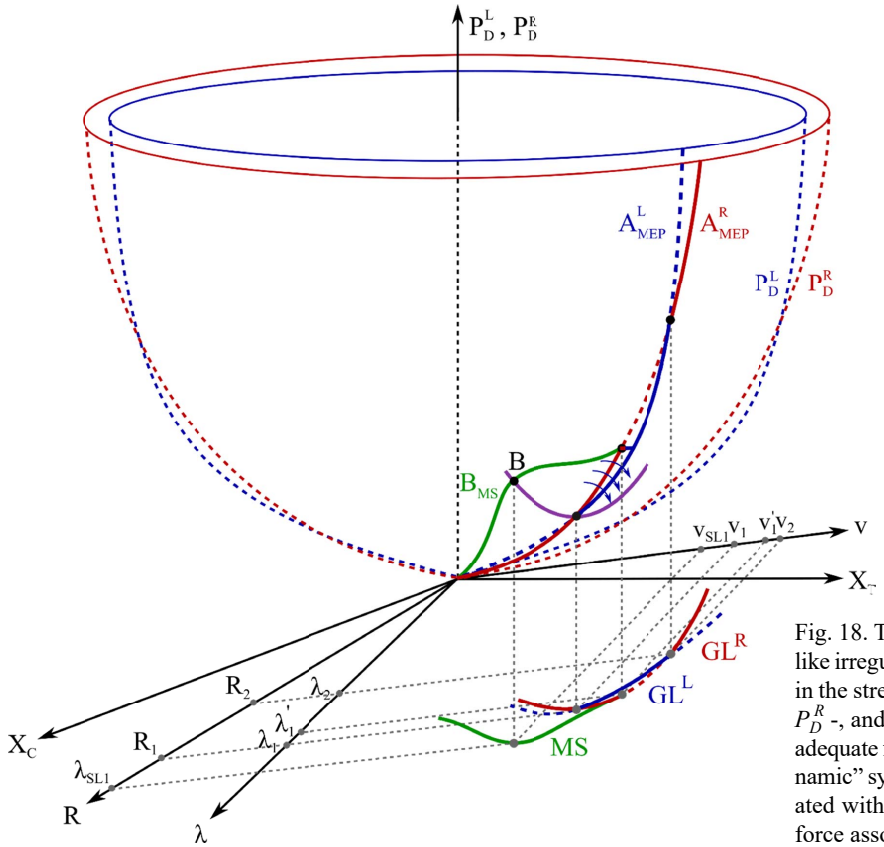

Fig. 18. Thermodynamic illustration for the formation of rod-like irregular structure, rod-like -, and lamellar regular structure in the strengthening layer of the (Zn) – single crystal; both the P_D^R -, and P_D^L – entropy production plotted as the paraboloids adequate for the X_T, X – primary coordinate system ("thermodynamic" system); X_T – generalized thermodynamic force associated with the heat transfer; X_C – generalized thermodynamic force associated with the mass transfer

The $\frac{\partial\left(P_D^L\right)}{\partial\lambda}\Big|_v = 0; \frac{\partial\left(P_D^R\right)}{\partial R}\Big|_v = 0$ – criteria (in the "technological" coordinate system) were applied to obtain some expressions for the *Growth Law*. However, the criteria can be used in minimization under condition that: $\min P_D^L(X_T, X_C) \Rightarrow \min P_D^L(v, S_\alpha + S_\beta)$, and $\min P_D^R(X_T, X_C) \Rightarrow \min P_D^R(v, r_\alpha + r_\beta)$, precisely. Thus, the following equation is to be satisfied in the current theory:

$$\frac{\partial P_D^L}{\partial X_T}\frac{\partial X_T}{\partial\left(S_\alpha + S_\beta\right)} + \frac{\partial P_D^L}{\partial X_C}\frac{\partial X_C}{\partial\left(S_\alpha + S_\beta\right)} = 0,$$
$$\frac{\partial P_D^R}{\partial X_T}\frac{\partial X_T}{\partial\left(r_\alpha + r_\beta\right)} + \frac{\partial P_D^R}{\partial X_C}\frac{\partial X_C}{\partial\left(r_\alpha + r_\beta\right)} = 0 \qquad (17)$$

The fulfilment of the above conditions, Eq. (17) has already been confirmed, [23]. On the other hand, the thermodynamics of irreversible processes provides the general criterion which is substantiated mathematically (the *Liouville's* theorem) for the stationary process itself: $\partial P/\partial X_C\big|_{X_T} = 0$.

The analyzed *Growth Law*, (developed in [4]), is general in form and is justified by the use of the criterion of *minimum entropy production*. The other versions of the *Growth Law* are also obtained, however, by the use of the intuitive condition of *minimum undercooling*, ΔT = min., [6]. The last mentioned theory shows the *Growth Laws* as follows:

$$\lambda^2 v = const_L. \text{ and } R^2 v = const_R. \qquad (18)$$

It can be proved that the version of the *Growth Laws*, Eq. (18), are, from the mathematical point of view, the particular case of the current *Growth Laws*, (developed in [4]). It means, that the current *Growth Law* is reducible to Eq. (18). Moreover, the mentioned reduction justifies the use of the intuitive condition of *minimum undercooling*, however, under certain restrictions only.

The application of the anisotropy of surface energies, [4], is an advantage of the current theory over those which had not taken it into a full account. Although both specific surface free energies vary across a lamellar width or rod-like radius in the interface, their values are characteristic / constant for the triple point for a given growth rate, and fulfil the parallelogram of vectors. These subtle capillary parameters, Fig. 14, play an essential role in the calculation of the entropy production and in the behavior of the entropy production examined in function of growth rate, Fig. 16. It is justified because the capillary parameters form the *s*/*l* interface curvature. The *s*/*l* interface curvature is taken into account in the calculation of the entropy production, [4], according to the requirements imposed by the mechanical equilibrium situated at the triple point of the *s*/*l* interface.

The minimization of the average entropy production, calculated in [4], according to Eq. (3), provides a possibility for the formation of a quite new version of the *Growth Law*.

Selection / application of the two conditions which are responsible for the creation of the whole spectrum of the interphase spacing, Fig. 4, allows to define the $v_{SL}^*(v^*) \Leftrightarrow v^*$ – *Operating Range* for the irregular structure formation.

The analyzed formation of the eutectic morphology proceeds according to the oscillation between stationary state and marginal stability, Fig. 17. The stationary state can be identified morphologically by the sinusoidal -, or parabolic shape of the *s*/*l* interface of the *non-faceted* phase. The sinusoidal shape is sometimes admitted, especially in the development of the formal description of the *s*/*l* interface curvature.

However, the parabolic shape seems to be typical of the regular eutectic structure, Fig. 3a, Fig 3c. The state of the marginal stability is identified by the wavy character of the maximally perturbed *s*/*l* interface of the *non-faceted* phase, Fig. 3b, Fig. 3c.

Calculation of the Ti – solute redistribution within the (Zn) – single crystal matrix, Fig. 7 visualizes that the material properties of the (Zn) – single crystal, as a whole, depend on the back-diffusion intensity during crystal growth, with the application of the definition: $0 \le \alpha \le 1$, Eq. (9).

The model for the solute redistribution, [24], illustrates that the width of the layer strengthening the single crystal also depends on the back-diffusion phenomenon, as explained in Eq. (12). It means that the back-diffusion controls the single crystal growth to a certain extent.

The leading phase protrusion, Fig. 3, and Fig. 13a, also seems to be essential for the resulting properties of the single crystal equipped with the strengthening layers. The observed protrusion appears in agreement with the theoretical prediction justified by the local mass balance, Fig. 11.

Contrary to the current model for the solute micro-field in the liquid adjacent to the s/l interface, [18], the mass balance is not satisfied in the former solution to the diffusion equation, [6]. The previous theory, [6], promotes the so-called *ideally coupled eutectic growth*, according to which, $\Delta T_\alpha = \Delta T_\beta$, whereas the present solution, [18], assumes the *coupled eutectic growth* only and the resultant inequality, $\Delta T_\alpha \neq \Delta T_\beta$, Fig. 12. This inequality, $\Delta T_\alpha \neq \Delta T_\beta$ is in harmony with the creation of the leading phase protrusion, Fig. 11.

The currently proposed description of the solute micro-field, [18], is the general theory, and therefore can be perfectly reduced (mathematically) to the previously provided model for the solute micro-field in the liquid, [6]. However, the reduction is possible under assumption that the width of the eutectic phases is equal to each other, $S_\alpha = S_\beta$. It means that the previous solution to the diffusion equation, [6], is associated with the virtual, symmetrical phase diagrams, only. Unfortunately, it is a significant restriction in the application of such a theory.

Thermodynamics of the irreversible processes requires the V – volume to be perfectly defined, [4], while integrating the entropy production per unit time and unit volume, Eq. (4). Moreover, the V – volume must contain the state of thermodynamic equilibrium, while the remaining part of this volume is under the deviation from this equilibrium. In the current model, the required deviation is defined in Fig. 12.

The present solution to the diffusion equation, Eq. (14), shows that the thermodynamic equilibrium is situated just at the

boundary between the liquid adjacent to the α – eutectic phase interface and that adjacent to the β – eutectic phase interface, that means, this state is situated at the elongation of the α/β – interphase boundary, Fig. 11. Thus, the V – volume contains the thermodynamic equilibrium as required. On the other hand, the s/l interface is under deviation from the thermodynamic equilibrium as expressed by Eq. (14).

A bifurcation from the plane s/l interface occurs when the v – growth rate is higher than the certain threshold rate, while the imposed thermal gradient is constant, [28]. The v_3 – rate, in the presented experiments, seems to be such a threshold rate for the appearance of the nonplanar pattern evolution. Then, the strengthening layer might become similar to the solitary wave (in the microscale), Fig. 19a.

This layer seems to present the initial pattern which evolves rapidly into cells. This phenomenon is known as the manifestation of the inherent instability that appears at the s/l interface, [29].

The mentioned non-planar pattern should be annihilated when the *Absolute Stability* of the *s/l* interface is ensured by an elevated growth rate imposed upon the *Bridgman's* system, and if the solute concentration is not subjected to any change, [30].

The above conclusion is confirmed by the current description of the solute micro-segregation and redistribution behavior for the growth rates greater than the v_{PS} – rate, Fig. 8, Fig. 9. An application of this description is successfully performed in the case of the D-gun spraying of the small particles onto the steel substrate (or water substrate) as developed in [25].

The solute concentration is neither subjected to any change when the partition ratio becomes equal to unity in the case of eutectic growth, [31].

The eutectic rod-like structure observed during stationary solidification, Fig 19a, appears periodically. Almost similarly, the Cu – Cu_2O – eutectic structure forms during copper droplets coagulation in the liquid slag. The eutectic is located at the every constituent droplets periphery, Fig. 13b, and Fig. 19b. The Cu – core of droplets plays a role similar to the (Zn) – matrix of the investigated single crystal. However, contrary to the (Zn) – matrix which presents the Ti – solute redistribution, Fig. 7, the droplets cores contains pure copper (100 at. %). This is in agreement with the adequate phase diagrams.

The eutectic layers reinforce the (Zn) single crystal, as mentioned. The Cu – Cu_2O – eutectic, Fig. 13b, Fig. 19b, increases the wettability and decreases the specific surface free energy of

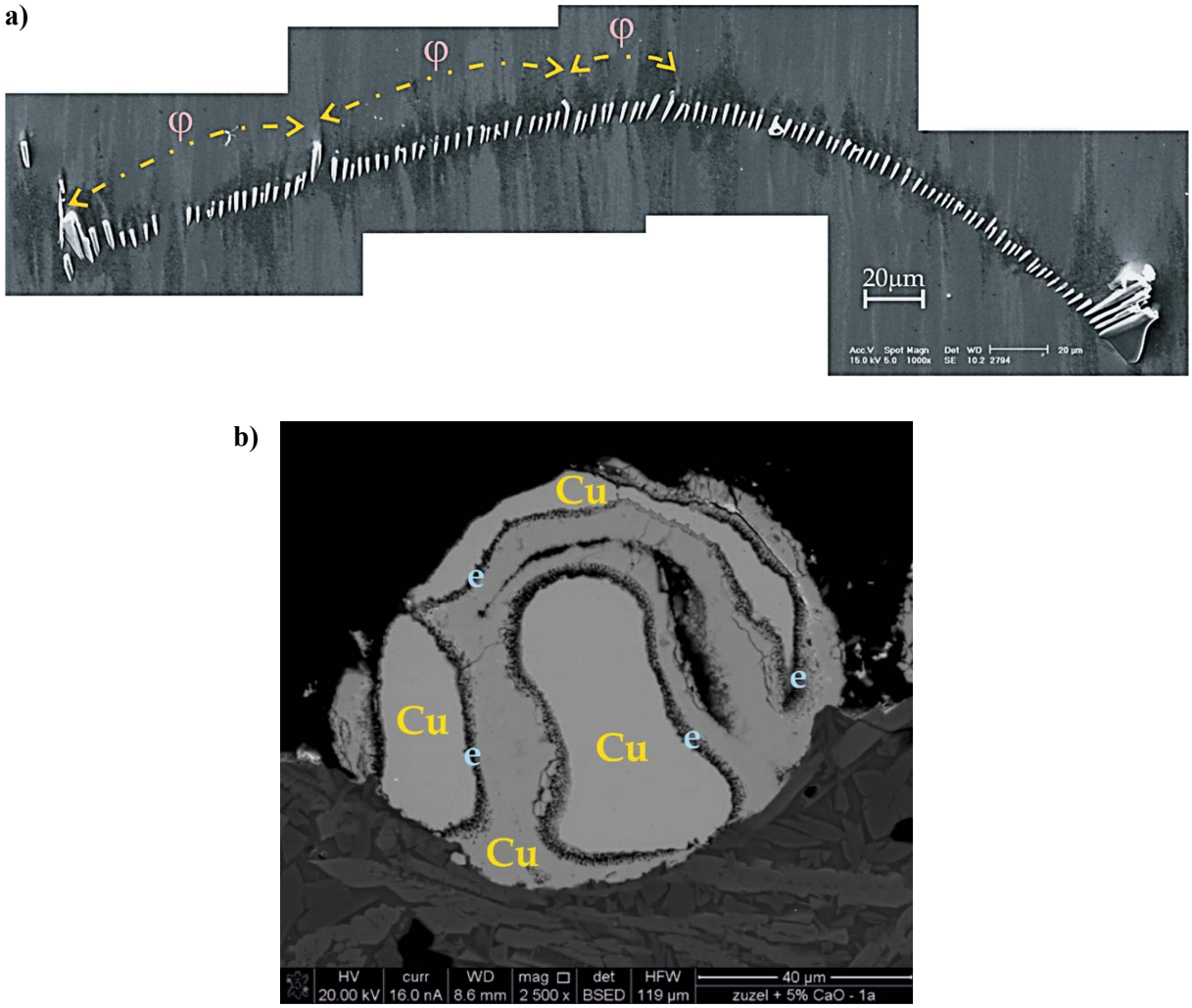

Fig. 19. Rod-like eutectic; a) strengthening layer observed within the (Zn) – single crystal for the $v > v_3$ – growth rate, b) Cu – Cu_2O – regular eutectic, (*e* – areas), accompanying the Cu – droplets coagulation

the copper droplet. As a result, the desired / required coagulation is easier. However, the coagulation is slightly more difficult when the lamellar eutectic precipitate appears.

REFERENCES

[1] G. Lesoult, M. Turpin, Memoires Scientifiques de la Revue de Metallurgie **66**, 619-631 (1969).

[2] W. Wołczyński, Archives of Metallurgy and Materials **63** (3), 1555-1564 (2018).

[3] M. Trepczyńska-Łent, Archives of Foundry Engineering **11** (2), 85-88 (2012).

[4] W. Wołczyński, Archives of Metallurgy and Materials **65** (1), 403-416 (2020).

[5] P. Glansdorff, I. Prigogine, Thermodynamic Theory of Structure, Stability and Fluctuations, Wiley – Interscience, a Division of John Wiley & Sons Ltd., London/UK – New York/USA – Sydney/ Australia – Toronto/Canada, (1971).

[6] K.A. Jackson, J.D. Hunt, Transactions of the Metallurgical Society of the AIME **236**, 1129-1142 (1966).

[7] W. Wołczyński, Crystal Research and Technology **25**, 1433-1437 (1990).

[8] G. Lesoult, Journal of Crystal Growth **13/14**, 733-738 (1972).

[9] B. Toloui, A. Hellawell, Acta Metallurgica **24**, 565-573 (1976).

[10] P. Magnin, W. Kurz, Acta Metallurgica **35**, 1119-1128 (1987).

[11] J.F. Major, J.W. Rutter, Materials Science and Technology **5**, 645-656 (1989).

[12] W.W. Mullins, R.F. Sekerka, Journal of Applied Physics **35**, 444-451 (1964).

[13] D.J. Fisher, W. Kurz, Acta Metallurgica **28**, 777-794 (1980).

[14] I. Prigogine, From Being to Becoming: Time and Complexity in the Physical Sciences, Ed. W.H. Freeman & Company, San Francisco/USA, (1980).

[15] E. Scheil, Zeitschrift fur Metallkunde **34**, 70-72 (1942).

[16] W. Wołczyński, Back-Diffusion Phenomenon during the Crystal Growth by the Bridgman Method, chapter 2 in the book: Modelling of Transport Phenomena in Crystal Growth, Ed. J.S. Szmyd & K. Suzuki; WIT Press: Southampton/UK – Boston/USA, 19-59 (2000).

[17] M.J. Aziz, Journal of Applied Physics **53**, 1158-1168 (1982).

[18] W. Wołczyński, Defect and Diffusion Forum **272**, 123-138 (2007).

[19] V.L. Davies, Journal of the Institute of Metals **93**, 10-14 (1964-65).

[20] G. Boczkal, Archives of Metallurgy and Materials **58** (4), 1019-1022 (2013).

[21] W. Wołczyński, Crystal Research and Technology **25** (12), 1433-1437 (1990).

[22] I. Prigogine, Introduction a la Thermodynamique des Processus Irreversibles, Monographies DUNOD, Paris/France, (1968).

[23] W. Wołczyński, Crystal Research and Technology **24**, 139-148 (1989).

[24] W. Wołczyński, Archives of Metallurgy and Materials **60** (3B), 2403-2407 (2015).

[25] W. Wołczyński, C. Senderowski, B. Fikus, A.J. Panas, Archives of Metallurgy and Materials **62** (4), 2391-2397 (2017).

[26] T. Himemiya, W. Wołczyński, Materials Transactions of the Japan Institute of Metals **43** (11), 2890-2896, (2002).

[27] P. Peng, X. Li, D. Liu, Y. Su, J. Guo, H. Fu, Acta Metallurgica Sinica, **49** (3), 311-319, (2013).

[28] B. Caroli, C. Caroli, B. Roulet, Journal de Physique **43**, 1767-1780 (1982).

[29] J.S. Kirkaldy, Metallurgical Transactions **24A**, 1689-1721 (1993).

[30] A. Ludwig, W. Kurz, Materials Science Forum **215-216**, 13-20 (1996).

[31] W. Wołczyński, Archives of Metallurgy and Materials **63** (1), 65-72 (2018).